Using Extended Kalman Filter for Data Assimilation and Uncertainty Quantification in Shock-Wave Dynamics

J. Kao, D. Flicker and R. Henninger
Los Alamos National Laboratory
kao@lanl.gov

M. Ghil and K. Ide
University of California at Los Angeles

Abstract

Model assimilation of data strives to determine optimally the state of an evolving physical system from a limited number of observations. The present study represents the first attempt of applying the extended Kalman filter (EKF) method of data assimilation to shock-wave dynamics induced by a high-speed impact. EKF solves the full nonlinear state evolution and estimates its associated error-covariance matrix in time. The state variables obtained by the blending of past model evolution with currently available data, along with their associated minimized errors (or uncertainties), are then used as initial conditions for further prediction until the next time at which data becomes available. In this study, a one-dimensional (1-D) finite-difference code is used along with data measured from a 1-D flyer plate experiment. The results demonstrate that the EKF assimilation of a limited amount of pressure data, measured at the middle of the target plate alone, helps track the evolution of all the state variables with reduced errors.

1. Introduction

Data assimilation has been used to estimate the state of a dynamic system by merging sparse data into a numerical model of the system [2, 4]. Based upon a prognostic model and a limited number of observations, data assimilation attempts to provide a more comprehensive system analysis which may lead to a better prediction. This approach has proven particularly fruitful recently in the atmospheric and oceanic sciences [2, 5].

The extended Kalman filter (EKF) method [2, 4, 5, 9, 10, 14] was designed to perform data assimilation with two stages: prediction and update. In the prediction stage, one solves the full nonlinear state evolution and, by using successive linearizations about the currently estimated state, advances the error covariance matrix in time. The update stage merges the model prediction and current observations, by

giving each appropriate weights, to provide an "analyzed" or "assimilated" state. These weights are obtained through minimizing the trace of the error-covariance matrix (i.e., the mean-square errors) based on a probabilistic analysis. The EKF thus provides a consistent first-order approximation to the optimal estimate of the nonlinear state at the observation time, as well as the errors of this estimate.

The current study investigates the performance of EKF for simple flyer plate experiments in a one-dimensional (1-D) set-up where most of its nonlinearity is fairly well understood [1, 16]. The numerical model we use in this study is the 1-D version of the MESA code (MESA-1D) [15].

EKF is a nonlinear extension of the Kalman filter [10, 11] in 1960 that had originally been developed for linear systems with a small number of model unknowns [4,12]. Its application to continuum-mechanics problems [2] requires substantial computer storage and a large number of operations [13]. The EKF has been used, therefore, in the atmospheric and oceanic sciences often for idealized problems [9, 14]. The current study, therefore, serves as a severe test in applying EKF for a realistic problem represented by a 1-D configuration in shock dynamics.

This paper is organized as follows. In Section 2 we give a brief review of the EKF method. Section 3 describes the MESA-1D code and the flyer plate experiments. Numerical results of applying EKF to actual experimental data appear in Section 4. Model uncertainties are discussed in Section 5. Concluding remarks appear in Section 6.

2. Extended Kalman Filter (EKF)

A detailed formulation of the EKF can be found in Gelb [4], Ghil and Malanotte-Rizzoli [5], Miller et al. [14] and Ide and Ghil [9]. A brief summary of the EKF method is given in this section.

The EKF first predicts the state variables $\mathbf{x}^f$ according to the system's deterministic equations, as a usual practice, where $\mathbf{x}$ is an N-

vector representing the state of the system (i.e., N is the number of the prognostic variables times the number of grid cells). The superscript 'f' stands for "forecast". The EKF then predicts the error-covariance matrix $\mathbf{P}^f$, defined by:

$$\mathbf{P}^f \equiv E \left[(\mathbf{x}^f - \mathbf{x}^t) (\mathbf{x}^f - \mathbf{x}^t)^T \right], \qquad (2.1)$$

where E represents the expectation operator, $\mathbf{x}^t$ represents the "true" state, and the superscript 'T' labels the transpose of a vector, using a matrix Riccati equation. The process described so far is straightforward and represents the EKF's prediction stage. The update stage is described below.

When observations become available, the EKF updates $\mathbf{x}^f$ and $\mathbf{P}^f$ to $\mathbf{x}^a$ and $\mathbf{P}^a$, respectively, where the superscript 'a' stands for "assimilated". Least-square minimization of $tr(\mathbf{P}^f)$, where tr is the trace of a matrix yields the Kalman gain matrix $\mathbf{K}$, which serves as a set of coefficient in weighting the so-called innovation vector, i.e. the difference between the actual observations and their model-predicted values.

The resultant $\mathbf{x}^a$ and $\mathbf{P}^a$ will be the initial conditions for the next cycle of prediction and update. The repetition of the prediction and update steps in time represents the sequential estimate of the system state and its uncertainties as obtained by the EKF. The performance of EKF can be measured by (1) evolution of $tr(\mathbf{P}^{f,a})$ that indicates the estimated least-square errors; (2) evolution of selected components of $\mathbf{P}^{f,a}$ that indicate how well the corresponding state variables are estimated in the least-square sense; and (3) comparison between the evolution of the observed and estimated state variables.

Both the system noise (or stochastic forcing) and solution errors due to numerical procedures and physical drawbacks have to be included in the prediction equation of $\mathbf{P}^f$ as given information. The solution errors may be determined by validation runs of the model against existing data [8] or by ensemble runs of the model against an ultra-high-resolution reference run [3]. In the current application, we combine both kinds of errors into one single term.

3. MESA-1D and Flyer Plate Experiment

The MESA-1D code uses the Eulerian conservation equations for mass, momentum, internal energy, and the Mie-Gruneisen equation of state (EOS). A third-order Van Leer's flux-limiting scheme for advection is used in order to maintain steep gradients without introducing large spurious oscillations. The material constitutive model for time-dependent deviatoric stresses is based on the classical elastic-perfectly-plastic treatment. The use of a ductile fracture (spall) model [1] is optional in the code.

The physical problem that we consider in this study is a 1-D flyer-plate experiment for which MESA-1D was used in a previous study [7]. A schematic diagram of the flyer-plate experiment is shown in Fig. 1. The flyer plate with a velocity of 0.0645 cm μs^{-1} (645m s^{-1}) and a thickness of 0.3 cm impacts the stationary target plate that is 6 times thicker. This produces a shock that compresses the material to a Hugoniot pressure of about 20 Gpa at the impact plane. The shock waves travel into both plates with a speed of about 0.45 cm μs^{-1}, estimated from the Hugoniot data. These waves eventually reach the other boundaries of the plates, where they reflect back into the plate interiors as rarefaction waves. When they meet again at about 4.7 μs, tensile forces occur and may cause spallation (ductile fracture) inside of the target plate [1].

4. Pressure Data Assimilation

In this section, we assimilate the pressure data measured from a flyer plate experiment into MESA-1D using the EKF method. For the current study, we have pressure data collected at the middle of the target plate by a Manganin pressure gauge between 2.0 to 3.8 μs (cf. Fig. 2). Therefore, most of the discussion regarding data assimilation with EKF is devoted to this time interval.

Figure 2 shows the evolution of pressure with time at the middle of the target plate, as obtained by several distinct approaches. The corresponding curves are color-coded and identified in the figure caption. The pure prediction without any data assimilation (blue dash-dotted curve) exhibits numerical ringing (the Gibbs phenomenon) along its flat top portion, between 2.0 and 2.5 μs, due to the higher-order advection scheme. The difference between this curve and the actual data (green curve) is obvious, especially during the release-wave interval, where the pressure starts to decrease with time. The result of assimilating the pressure data with the EKF (solid black curve) agrees rather well with the data points in green. The result suggests that, with the given observation and model errors, the data carries

more weight in the optimization process than the model. It even overcomes the numerical ringing during the flat top interval.

Note in Fig. 2 that there are three distinct time intervals with no data available: (i) 2.25 to 2.5 μs, (ii) 2.7 to 2.9 μs, and (iii) 3.1 to 3.45 μs. During each of these intervals, the model run with EKF is essentially making a prediction, based upon the updated information at the beginning of the interval, until the next update. For the first two intervals, the model run with EKF does a credible prediction, as verified by comparing the prediction and the data points near the end of the time intervals.

As for the last interval that data are not available, the model run with EKF does not lead to a close matching of the next available data; instead, it coincides with the pure prediction as a result of the very similar initial conditions between the two cases during this interval. The sudden restoring feature at the end of this interval in the black curve shows that the EKF has very high confidence in the data. The further zig-zag variation in the black curve (from 3.5 to 4.0 μs) reflects the same situation. Namely, the prediction made by the EKF run between updates tends to stay away from the data until it is pulled back by the update process at each observation time.

It is clear from the above discussion that the pure prediction has a systematically sharper fall-off in pressure than the experimental data during the release-wave interval. As a result of applying data assimilation, the predicted pressure with EKF at the end of the simulation is about 12 kbar higher than the pure prediction. An additional simulation was made in which no more data points were used after the update at 3.4 μs (red dashed curve). This prediction for the rest of the simulation gradually merges to the blue dash-dotted curve that represents the pure prediction for the entire interval.

Figure 3 shows the effects of data assimilation with the pressure data on all the state variables: density, velocity, and internal energy at the middle of the target plate; pressure is repeated here for reference purposes. Pressure is not considered as a state variable and is a given function of density and internal energy; i.e., equation of state. As a result, these two state variables are affected by the assimilation of pressure data in a similar way as pressure itself is, especially over the flat-top interval. Due to the lack of an explicit dependence of pressure on velocity, the velocity field is affected less by the data assimilation, inasmuch as the difference between the pure prediction (blue dash-dotted curve) and the EKF run (solid black curve) is smaller.

Even though pressure was measured and assimilated only at the middle of the target plate, the effects of data assimilation are definitely not limited to this point, as shown in Fig. 4. This figure represents the averaged effects of EKF over the whole material domain. The results thus confirm the main virtues of the EKF for the highly nonlinear physics of shock-wave dynamics: (i) information trade-off between observed variables and unobserved; and (ii) propagation of information by the governing equations, from observed to unobserved locations [2, 5, 6].

5. Evolution of Uncertainties

As emphasized in Section 2, EKF performance can also be measured by the error covariance matrices. Figure 5 shows the global error with and without the EKF process. Due to the magnitude difference among the three state variables (cf. Fig. 6), $tr(\mathbf{P}^f)$ is entirely dominated by the variances of density. Until data become available at 2.0 μs, the pure prediction results (blue dash-dotted curve) and those with data assimilation (black solid curve) coincide. The initial sudden drop in $tr(\mathbf{P}^f)$ shows merely that the initial value of $\mathbf{P}^f$ was estimated too large by a factor of 3. After this initial adjustment of about 0.5 μs, the mean-square error increases slowly, with an approximately constant slope, due to the additive stochastic model error.

When the pressure data become available, the mean-square error drops again suddenly, but only in the EKF run (black curve). During the interval of data availability, between 2.0 μs and 3.8 μs, the assimilation results have the same overall upward trend as the pure prediction results (blue curve), but run systematically lower and drop slightly each time when the pressure data becomes available. This shows that a single scalar observation can noticeably reduce the error in estimating the state of our system, with its total number of 222 discrete variables.

Figure 6 shows the variances for each individual state variable at the middle of the target plate as a function of time; these variances are simply the diagonal entities of $\mathbf{P}^f$ at the appropriate grid point. Taking the square root of the values in Fig. 6 essentially provides error bars for Fig. 3. Each state variable in Fig. 6 carries a maximum variance near 2.0 μs for the pure prediction case, suggesting that the

shock arrival (cf. Fig. 3) must significantly increase model errors in the system at hand. The data point of pressure near 1.9 μs effectively reduces the density variance from a maximum to nearly zero. A similar effect is seen in the internal energy variance. Due to the dependencies of pressure on density and internal energy, the variances of these two state variables at each up time are characterized by distinct but small-amplitude fluctuations.

6. Concluding Remarks

The extended Kalman filter (EKF) method [5, 9, 10, 14] was employed in the current study for assimilating data into the MESA-1D code [15]. EKF was designed to optimize predictions of, as well as reduce uncertainties in, the modeled state variables, provided that the errors of observations and model performance are known. The EKF algorithm solves the full nonlinear state evolution and its associated error-covariance matrix in time. It provides a consistent first-order approximation to the optimal estimate of the state and of the time-dependent model uncertainties, both when data are available and when they are not.

A limited amount of experimental data was available for this study from a 1-D flyer plate experiment (Fig. 1). The EKF results, in general, demonstrate that pressure data at the middle of the target plate alone helps track the evolution of all the state variables (Figs. 2 to 6). After the model update at observation time, the "assimilated" state variables and their associated minimized errors are used as initial conditions for a fresh start of model prediction till the next data time, or, if data is no longer available, till any desired future time. For shock-wave related research or applications, the EKF thus provides important additional information where experimental data are missing, in part or altogether.

To the best of our knowledge, there has been no previous attempt to use data assimilation in high-speed impact studies or solid mechanics modeling. We have shown here how this approach can expand and refine our knowledge in these fields using the limited laboratory data available. Using the same methodology, we expect to use the EKF for the optimal estimation of physical parameters in future applications.

ACKNOWLEDGMENTS

References

[1] Addessio, F. L., and J. N. Johnson, 1993: Rate-dependent ductile failure model. J. Appl. Phys., 74, 1640-1648.

[2] Bengtsson, L., M. Ghil, and E. Källén (Eds.), l98l: Dynamic Meteorology: Data Assimilation Methods, Springer-Verlag, New York/Heidelberg/Berlin, 330 pp.

[3] DeVolder, B., J. Glimm, J. W. Grove, Y. Kang, K. Pao, D. H. Sharp, 2002: A statistical study of errors in simulations of shock wave interaction. Los Alamos Unclassified Release. LA-UR-01-3671.

[4] Gelb, A. (Ed.), 1974: Applied Optimal Estimation. The MIT Press, 347pp.

[5] Ghil, M., and Malanotte-Rizzoli, P., 1991: Data assimilation in meteorology and oceanography. Adv. Geophys., 33, 141-226.

[6] Ghil, M., 1997: Advances in sequential estimation for atmospheric and oceanic flows. J. Meteor. Soc. Japan, 75, 289–304.

[7] Henninger, R. J., P. J. Maudlin, and M. L. Rightley, 1997: Accuracy of differential sensitivity for one-dimensional shock problems. APS Shock Compression of Condensed Matter Conference, Amherst, MA.

[8] Hills, G. R., and T. G. Trucano, 2001: Statistical validation of engineering and scientific models with application to CTH. Sandia National Laboratory Rep., SAND2001-0312, 118pp.

[9] Ide, K., and M. Ghil, 1997a: Extended Kalman filtering for vortex systems. Part I: Methodology and point vortices. Dyn. Atmos. Oceans, 27, 301-332.

[10] Jazwinski, A. H., 1970: Stochastic Processes and Filtering Theory, Academic Press, New York, 376 pp.

[11] Kalman, R. E., 1960: A new approach to linear filtering and prediction problems. Trans. ASME, Ser. D, J. Basic Eng., 82D, 35-45.

[12] Kalman, R. E., and R. S. Bucy, 1961: New results in linear filtering and prediction problems. Trans. ASME, Ser. D, J. Basic Eng., 83D, 95-108.

[13] Lyster, P. M., S. E. Cohn, R. Menard, L.-P. Chang, S. –J. Lin, and R. Olsen, 1997: Parallel implementation of a Kalman Filter for constituent data assimilation. Mon. Wea. Rev., 125, 1674-1686.

[14] Miller, R., Ghil, M., Gauthiez, F., 1994: Advanced data assimilation in strongly nonlinear dynamical systems. J. Atmos. Sci., 51, 1037-1056.

[15] Cagliostro, D. J., D. A. Mandell, L. A. Schwalbe, T. F. Adams, and E. J. Chapyak, 1990: MESA 3-D calculations of armor penetration by projectiles with combined obliquity and yaw, Int. J. Impact Engineering, 10.

[16] Zukas, J. A. (Ed.), 1990: High Velocity Impact Dynamics. John Wiley & Son Press, 935pp.
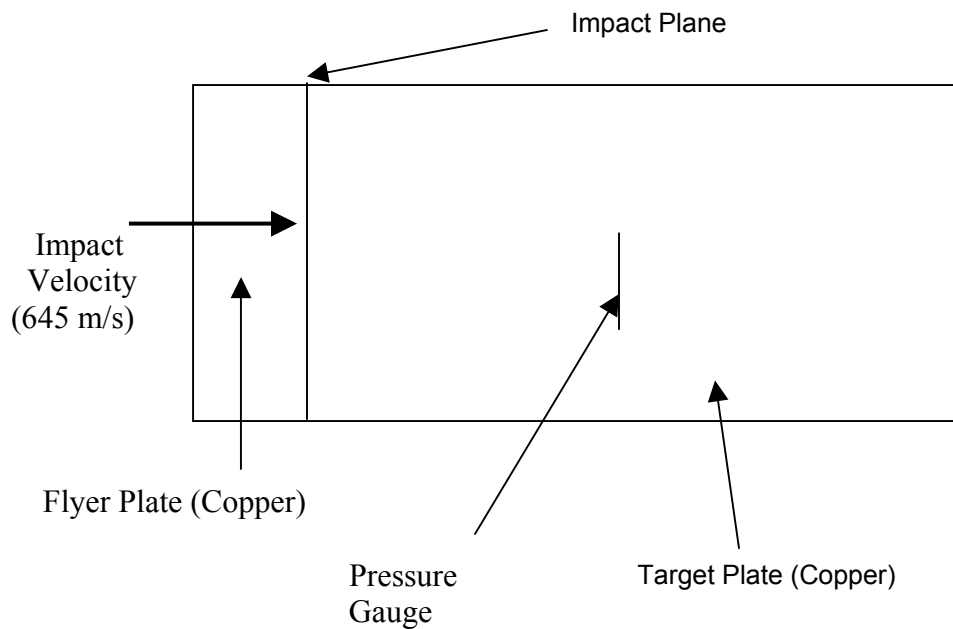
Fig. 1. A schematic diagram of the 1-D flyer plate experiment.
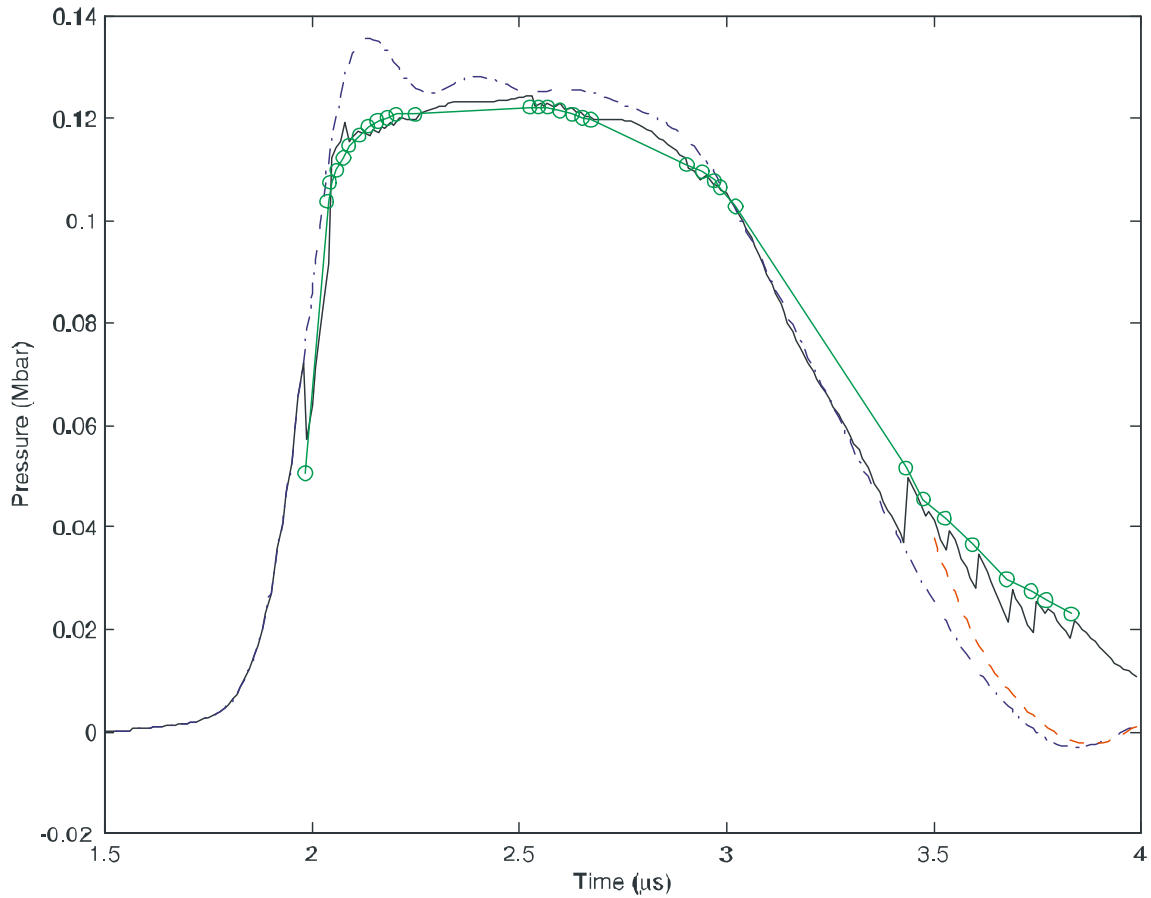
Fig. 2. Pressure evolution at the middle of the target plate with an observation error (w) of 0.1 kbar and a normalized model error (q) of 0.001. Green curve: fitted to the experimental data points marked by green circles; blue dash-dotted curve: pure prediction without EKF; black solid curve: assimilated evolution with EKF; red dashed curve: the evolution that the black curve would have undergone if no data were available after 3.4 μs.
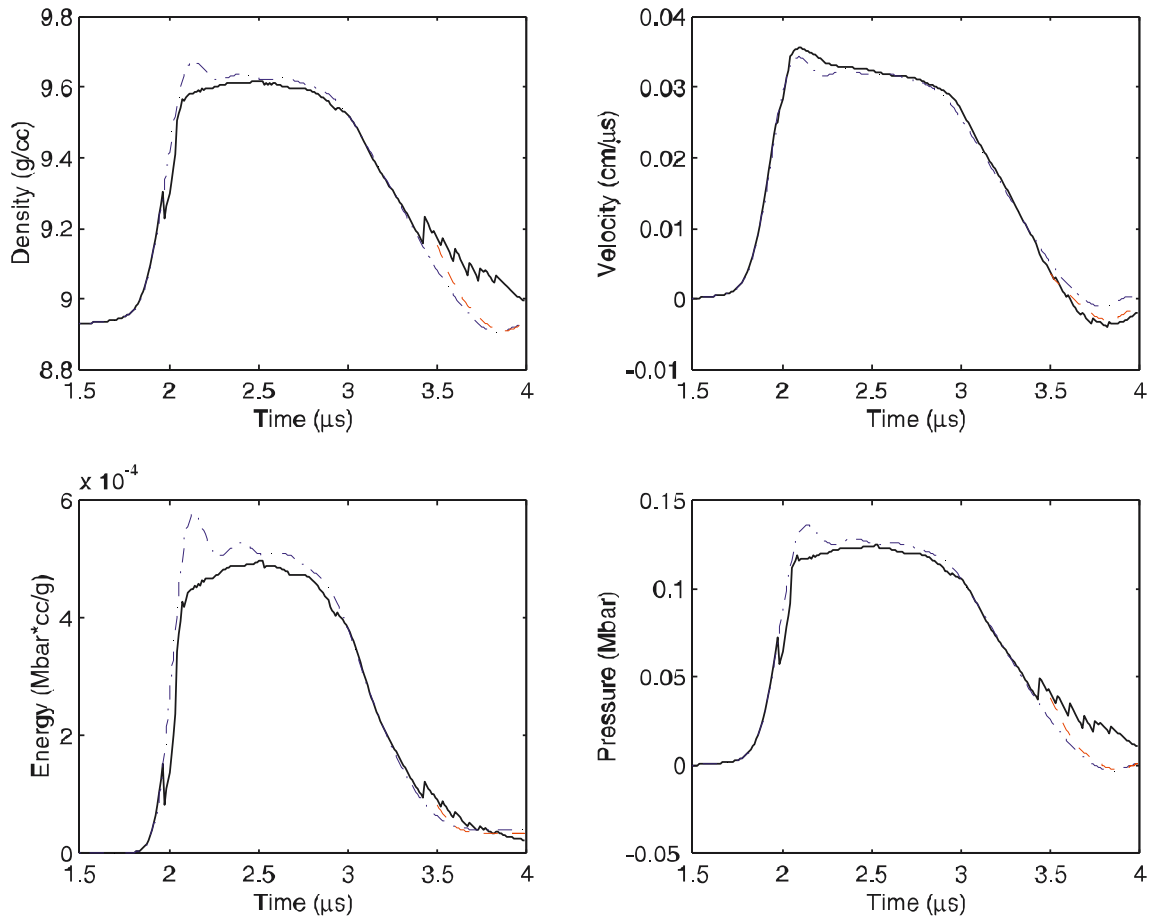
Fig. 3. Time evolution of all the state variables (density, velocity, and internal energy) and the pressure for the same simulation and at the same location as depicted in Fig. 2. Refer to Fig. 2 for curve legends.
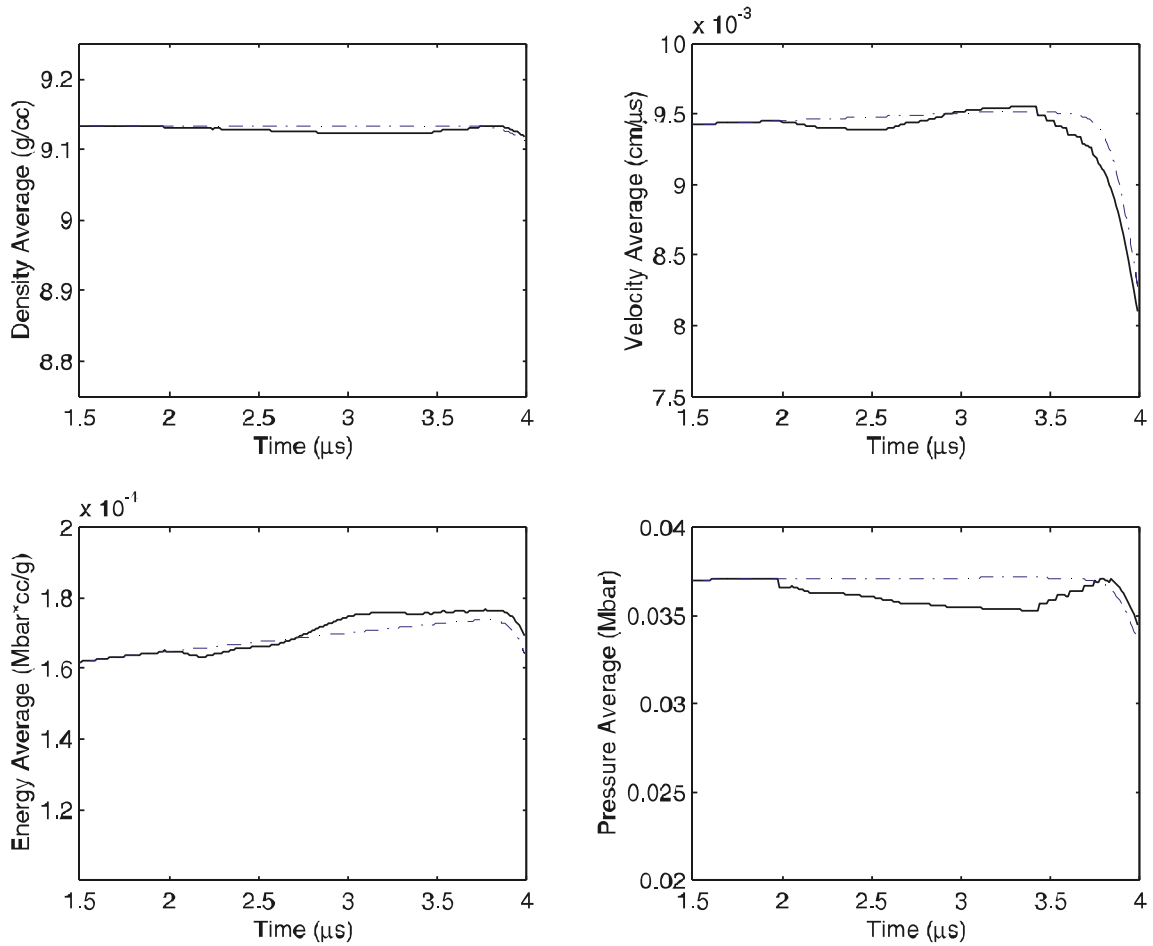
Fig. 4. The same as Fig. 3 except for spatially averaged time evolution over all material grid points. Blue dash-dotted curve: pure prediction without EKF; and black solid curve: assimilation with EKF.
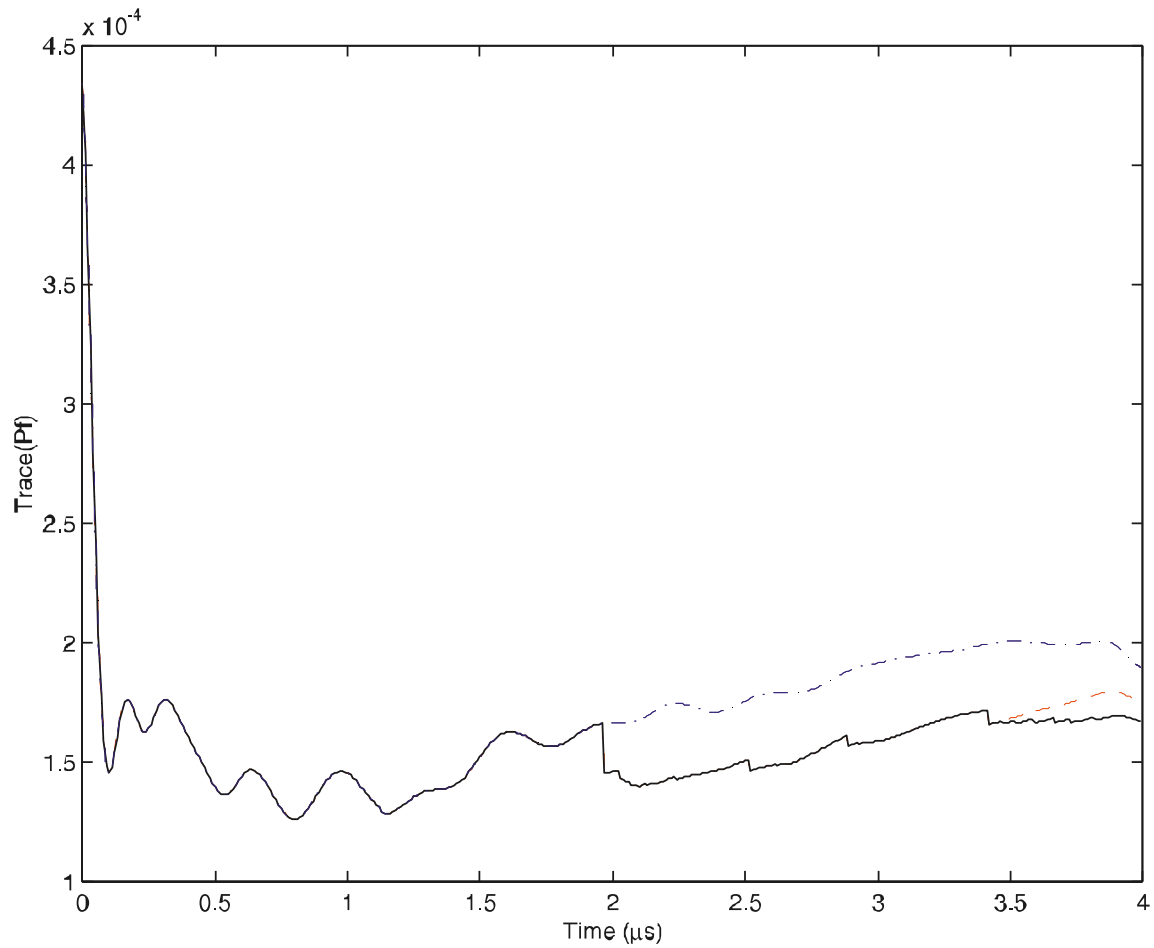
Fig. 5. The trace of $\mathbf{P}^p$ (the sum of the variances) as a function of time. Blue dash-dotted curve: pure prediction without EKF; black solid curve: assimilated evolution with EKF; red dashed curve: the evolution that the black curve would have undergone if no data were available after 3.4 μs. The blue and black curves coincide with each other until the first data point at 1.9 μs.
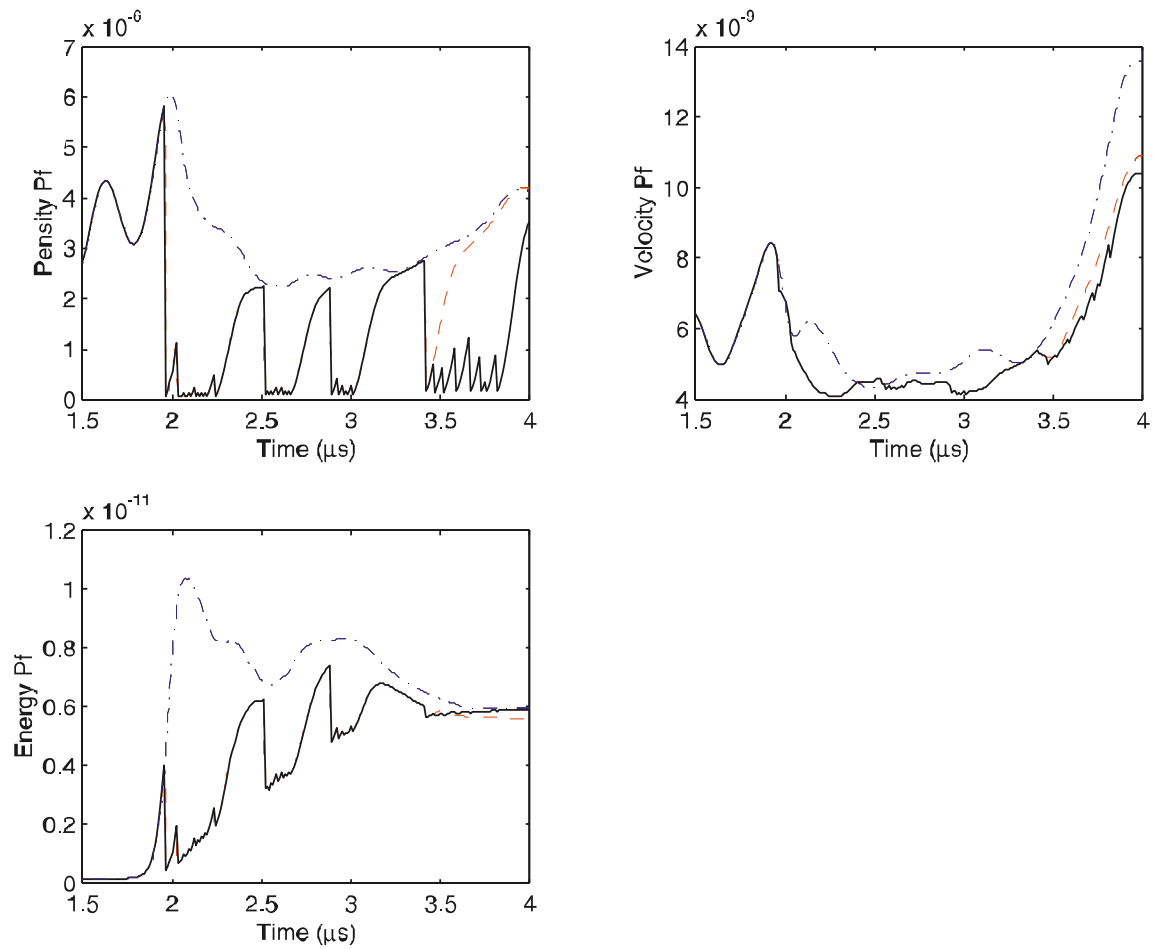
Fig. 6. The variances of the three state variables at the middle of the target plate as a function of time. Refer to Fig. 5 for the legends of different curves.